Microstructure and Properties of a Novel Nickel-Based Corrosion-Resistant Alloy Welded Joint (Postprint)

Authors: Zhao Xia, Xiangdong Zha, Zhang Long, Liang Tian, Yingche Ma, Liu Kui

Date: 2016-11-04T00:00:00+00:00

Abstract

Through tensile property and hardness testing of manual tungsten inert gas (TIG) welded joints of a novel nickel-based corrosion-resistant alloy (X-2#), combined with OM, SEM, and EDS techniques, the microstructure and properties of the welded joints were systematically investigated. The results indicate that the weld zone of the X-2# alloy welded joint exhibits as-cast microstructure, the fusion zone shows a good transition from base metal to weld metal microstructure, the heat-affected zone does not exhibit obvious grain coarsening, and the base metal grain size of grade 5 is beneficial for welding of the joint. The Vickers hardness value of the weld zone in the new alloy is lower than that of the base metal, but the Vickers hardness value of the weld remelting zone increases due to the increased number of equiaxed grains. The solid solution strengthening elements such as W and Mo, as well as the precipitation strengthening elements Al and Ti in the alloy, endow the X-2# alloy welded joint with good high-temperature strength and thermal stability. The tensile strength of the alloy welded joint at both room temperature and high temperature is lower than that of the base metal, the welding coefficient is greater than 88%, the weld zone is the weakest link of the joint, all tensile fracture surfaces are ductile fractures, and the fracture mechanism is a mixed fracture of normal fracture and shear fracture.

Full Text

Microstructure and Properties of Welding Joints of a New Corrosion-Resistant Nickel-Based Alloy

Authors: Zhao Xia[1], Liu Yang[2], Zha Xiangdong[3], Cheng Leming[2], Ma Yingche[3], Liu Kui[1]

[1] College of Materials and Metallurgical Engineering, Northeastern University, Shenyang 110819
[2] ENN Science & Technology Development Co. Ltd., Langfang 065001
[3] Institute of Metal Research, Chinese Academy of Sciences, Shenyang 110016
Corresponding Author: Ma Yingche, associate professor, Tel: (024)23971986, E-mail: ycma@imr.ac.cn

Abstract: The tensile properties and hardness of manual argon tungsten arc welding joints of a new nickel-based corrosion-resistant alloy (X-2#) were tested, and the microstructure and properties of the welding joints were investigated using optical microscopy (OM), scanning electron microscopy (SEM), and energy-dispersive spectroscopy (EDS). The results show that the weld zone of the X-2# alloy welding joint exhibits a cast structure. The fusion zone demonstrates a smooth transition from the base metal to the weld metal, and the heat-affected zone (HAZ) shows no significant grain coarsening. The base metal has a grain size of grade 5, which is favorable for weldability. The Vickers hardness of the weld zone is lower than that of the base metal, but the hardness of the weld remelting zone increases due to a higher number of equiaxed crystals. The solid solution strengthening elements W and Mo, together with the precipitation strengthening elements Al and Ti, endow the X-2# alloy welding joint with good high-temperature strength and thermal stability. The tensile strength of the welding joint is lower than that of the base metal at both room temperature and elevated temperatures, with a welding coefficient greater than 88%. The weld zone represents the weakest link of the joint, and all tensile fractures are ductile, exhibiting a mixed fracture mechanism of normal fracture and shear fracture.

Keywords: Nickel-based corrosion-resistant alloy, weld zone, fusion zone, heat-affected zone

---

Introduction

With the rapid development of China' s industry, industrial organic wastewater has become increasingly characterized by high concentration, complex composition, and difficulty in degradation. Conventional wastewater treatment technologies can no longer meet the requirements, and supercritical water oxidation (SCWO) has gained extensive attention and application in wastewater treatment due to its technical and economic advantages [1~3]. However, this method requires operation under high temperature, high pressure, strong corrosion, and oxidation conditions, demanding exceptional performance from container components and materials, particularly in terms of high-temperature, high-pressure, and corrosion resistance. The primary constraint on this technology' s application is the poor corrosion resistance and processability of materials used in treatment equipment, resulting in short service life [4,5]. The problem is especially pronounced for preheater or reactor piping materials, where preheating

temperatures range from 300–500 °C at 25 MPa, and reaction temperatures reach 550–650 °C at 25 MPa. Therefore, developing new corrosion-resistant materials for supercritical water oxidation environments holds significant scientific importance and application value.

Materials for preheaters or reactors in supercritical water environments typically require high creep strength, strong resistance to steam oxidation and corrosion, excellent processability, and economic viability. Current research on materials primarily focuses on ferritic/martensitic (F/M) steels, oxide dispersion strengthened (ODS) steels, austenitic stainless steels, and nickel-based alloys. The corrosion of F/M steels in supercritical water deteriorates with increasing temperature and dissolved oxygen, exhibiting substantial weight gain, thick oxide layers, and accumulation of high internal stresses that lead to cracking and porosity of the surface oxide film [6~13]. Although the weight gain follows the parabolic law of protective oxide films, their corrosion resistance is generally considered poor. ODS steels typically exhibit better overall corrosion resistance than comparable F/M steels, but this depends heavily on specific elemental composition. High-Cr ODS steels show good corrosion resistance, while low-Cr ODS steels generally perform poorly, forming oxide films similar to those of F/M steels [14~18]. Austenitic stainless steels demonstrate good corrosion resistance in low-temperature supercritical water but are prone to oxide spallation and large-scale non-uniform corrosion at high temperatures, though their overall corrosion resistance is superior to that of F/M steels [19~22]. Nickel-based alloys exhibit minimal weight gain in supercritical water, especially at high temperatures, but show large fluctuations in corrosion weight gain and are susceptible to non-uniform corrosion such as spallation, pitting, and oxide particles [23~25]. Considering all factors, nickel-based alloys are the most promising candidate materials for supercritical environments [26]. Consequently, a new nickel-based alloy X-2# containing 10% Fe (mass fraction) has been successfully developed, demonstrating excellent high-temperature strength, ductility, and microstructural stability, with virtually no oxidation at 760 and 1000 °C, superior high-temperature oxidation resistance, and better corrosion resistance under supercritical conditions in PO^{3}-dominated environments compared to alloys 671, C-276, and 625. This work investigates the microstructure and mechanical properties of welded joints of the new nickel-based corrosion-resistant alloy X-2# to provide reliable theoretical data support for future applications.

Experimental Materials and Methods

The chemical composition of the new nickel-based corrosion-resistant alloy X-2# used for welding experiments is (mass fraction, %): C 0.01, Cr 20.0, Mo 1.0, Al 1.0, W 4.0, Fe 10.0, Ti 1.0, Ni balance. The new alloy was vacuum induction melted, forged, and hot-rolled into plates before undergoing solution heat treatment. The base metal for welding was in the solution-treated condition, with a solution treatment regime of 1120 °C for 30 min followed by water quenching. The welding process was manual tungsten inert gas (TIG) welding

using double-sided welding with X-2# alloy filler wire and an X-shaped groove. The welding current was 110–120 A for both front and back sides, with welding speeds of 130–140 mm/min for the front side and 150–160 mm/min for the back side. Shielding gas flow was 20 L/min for the torch and 10 L/min for backside protection.

Samples were cut perpendicular to the welding direction using wire electrical discharge machining and mechanically polished on one side perpendicular to the welding joint. A solution of 18 mL H SO + 4 g K MnO + 180 mL H O was used as an etchant. Samples were boiled in the etchant for 30 min, then cleaned with oxalic acid solution, rinsed with alcohol, and dried. Microstructure observation was performed using an Observer.Z1m optical microscope (OM). Microhardness measurements were conducted using an LM247AT automatic digital Vickers microhardness tester with a load of 300 g and dwell time of 15 s. Measurement positions are shown by the dashed lines in [FIGURE:1], with hardness values taken every 0.7 mm. Tensile specimen dimensions are shown in [FIGURE:2]. Tensile tests were performed at room temperature (20 °C), 300, 400, 500, 600, and 700 °C, with three samples tested at each temperature and average values reported. Tensile testing was conducted on an AG-5000A DCS-25T testing machine, and microstructure and fracture morphology were observed using an S-3400N scanning electron microscope (SEM).

Results and Discussion

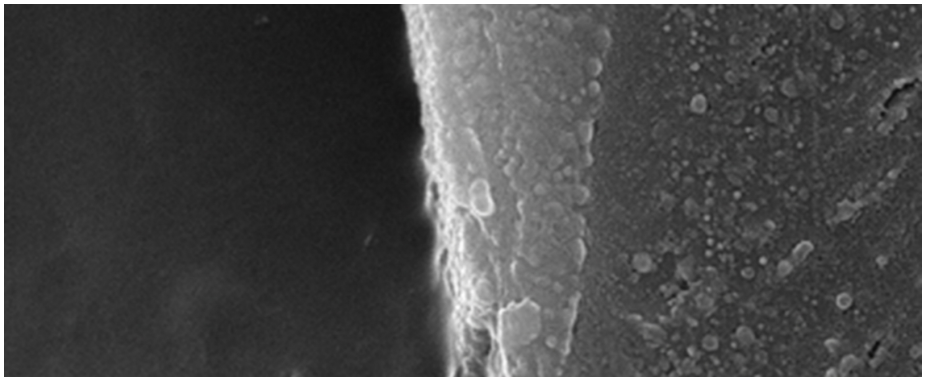

Figure 1: Figure 3

2.1 Microstructure shows the microstructure of the X-2# alloy welding joint. As seen in [FIGURE:3a], the X-2# alloy base metal exhibits a typical fully austenitic equiaxed grain structure with numerous twin boundaries and relatively straight grain boundaries, with a grain size of grade 5. [FIGURE:3b] indicates that the weld zone of the X-2# joint displays a continuous cooling cast structure, where the bottom edge near the base metal shows epitaxial growth. During welding cooling, the weld grows inward from locally semi-melted grains

on the fusion line in the direction of fastest heat dissipation, forming highly directional columnar crystals, while the top region consists of equiaxed crystals. The formation of equiaxed crystals is related to cooling rate; rapid cooling creates high undercooling, causing the temperature at the weld top to drop below the crystallization temperature and nucleate before the bottom columnar crystals reach the top, resulting in freely grown equiaxed crystals.

In double-sided welding, the backside welding is performed after the front side welding, creating an overlapping region known as the weld remelting zone, which is also part of the weld zone. [FIGURE:3c] shows that the X-2# alloy weld remelting zone exhibits reduced columnar crystal structure and increased equiaxed crystal structure in the bottom region, primarily because the bottom region of the front weld undergoes a secondary thermal cycle from the backside welding, promoting secondary dendrite growth. The fusion zone is the transition region between the weld zone and heat-affected zone, sometimes called the fusion line. [FIGURE:3d] demonstrates that the X-2# alloy welding joint fusion zone shows a smooth transition from base metal to weld metal, with a clear and distinct fusion zone free from defects such as cracks, porosity, and inclusions, indicating good welding quality. As shown in [FIGURE:3e], the heat-affected zone microstructure shows no significant grain coarsening compared to the base metal, indicating strong thermal stability of the new alloy. The degree of grain growth in the HAZ depends on the original grain size of the base metal and welding heat input. If the base metal has small grains and experiences high welding heat input and pre-weld plastic deformation, significant grain growth occurs. Conversely, if the base metal has large grains and minimal original plastic deformation, grain growth remains limited even under high heat input conditions. When welding heat input is low and the temperature gradient is steep, even small grains may coarsen significantly [27]. The X-2# base metal has a grade 5 grain size, and no obvious grain growth was observed in the HAZ, indicating that the grain size and welding heat input are appropriately matched for the X-2# alloy.

2.2 Microhardness Distribution [FIGURE:4] presents the Vickers hardness distribution across the X-2# alloy welding joint. The base metal hardness is higher than that of both front and back weld zones, and the HAZ hardness transitions smoothly between the weld zone and base metal without significant fluctuations, as shown in [FIGURE:4a] and [FIGURE:4b], because the HAZ microstructure remains stable without obvious grain growth. [FIGURE:4c] indicates that the hardness of the double-sided weld remelting zone is similar to that of the base metal. At the center of the weld zone, the hardness of the double-sided weld remelting zone exceeds that of both front and back weld zones ([FIGURE:4d]), because the remelting zone effectively undergoes a tempering heat treatment on the front weld microstructure, reducing brittleness and increasing ductility and toughness while stabilizing the microstructure to achieve a good combination of strength and toughness. In summary, the X-2# alloy welding joint exhibits higher hardness in the base metal than in the weld zone,

with the weld zone being the softest region, but the weld remelting zone shows higher hardness than both front and back weld zones and approaches the base metal hardness.

2.3 Tensile Properties and Fracture Behavior

2.3.1 Tensile Testing [FIGURE:5] shows the morphologies of X-2# alloy welding joints after tensile testing at various temperatures. The results indicate that after tensile testing at room temperature (20 °C) and elevated temperatures (300, 400, 500, 600, and 700 °C), all specimens fractured in the weld zone through ductile fracture, demonstrating that the tensile strength of the X-2# welding joint is lower than that of the base metal. Since ductile fracture involves slip before fracture, the fracture surfaces are uneven with shear lips at 45° angles to the principal stress direction. The figure also reveals necking in each tensile specimen, with slight plastic deformation occurring in the base metal on both sides of the weld.

presents the tensile test data for X-2# alloy welding joints at different temperatures. The results show that the tensile strength of X-2# alloy welding joints is lower than that of the base metal at both room temperature (20 °C) and elevated temperatures (300, 400, 500, 600, and 700 °C), with fracture occurring in the weld zone. When the tensile temperature increases from room temperature (20 °C) to 300 °C, the tensile strength of both the X-2# alloy base metal and welding joints decreases by approximately 80–100 MPa. With further temperature increase, the strength reduction becomes smaller; when temperature rises from 600 °C to 700 °C, the tensile strength of both base metal and welding joints decreases by only about 3–30 MPa. The excellent high-temperature strength of X-2# alloy is attributed to the addition of age-hardening elements Al and Ti, which cause the precipitation of ’ strengthening phase at 700 °C, thereby enhancing alloy strength. also reveals that the welding coefficient of X-2# alloy welding joints remains relatively stable between 92% and 95%, though it decreases slightly to 88.1% at 700 °C. Nevertheless, under the previously mentioned service temperature and pressure conditions, the joint strength and weldability of X-2# alloy remain stable and can meet application requirements.

2.3.2 Fracture Morphology [FIGURE:6] shows the fracture morphologies of X-2# alloy welding joints after tensile testing at different temperatures. As seen in [FIGURE:6a]–[FIGURE:6c], the fracture surfaces at 20, 200, and 300 °C exhibit dimpled features characteristic of ductile fracture. With increasing test temperature, the dimples become shallower, smaller, and less uniform, indicating reduced ductility and toughness. [FIGURE:6d]–[FIGURE:6f] show that fracture surfaces at 500, 600, and 700 °C display mixed ductile fracture morphologies consisting of dimples and tear ridges. As test temperature increases, the tear ridges become larger and more numerous, reflecting good high-temperature strength.

2.3.3 Fracture Mechanism The fracture mode of welding joints is related to different void expansion mechanisms in the joint microstructure during tensile testing, which in turn depends on the stress state experienced by the joint. To concisely and efficiently reflect the stress state of loaded components, the concept of stress triaxiality (R) is generally introduced [28~29], expressed as:

$$R_{\sigma} = \frac{\sigma_m}{\sigma_{eq}} = \frac{\sigma_1 + \sigma_2 + \sigma_3}{3\sigma_{eq}}$$

where , , are principal stress components, is mean stress, and q is equivalent stress. During high-temperature tensile testing, R typically has two critical values, R and R , with R > R . Dimple formation results from local plastic deformation that first creates microcracks at second-phase particle interfaces (inclusions), which then expand ([FIGURE:7]). A "internal necking" occurs in the local region between inclusions and the matrix metal, and when the necking reaches a critical level, tearing or shear fracture occurs, creating the dimple fracture morphology [30]. Depending on the stress state, dimples can be categorized as either normal fracture dimples or shear fracture dimples. Under normal stress, R is relatively large (R > R), with uniform stress distribution across the fracture surface, causing microvoids perpendicular to the principal stress to grow uniformly in all directions and form equiaxed dimples (normal fracture) with minimal plastic deformation. Under shear and tearing stresses, R is relatively small (R < R < R), with non-uniform stress distribution during void nucleation and growth, resulting in non-uniform deformation and parabolic-shaped dimples (shear fracture) with increased plastic deformation [29~30]. As shown in [FIGURE:6], the tensile fracture surfaces of X-2# welding joints at different temperatures exhibit both equiaxed dimples and parabolic dimples with tear ridges, indicating a mixed fracture mechanism of normal fracture and shear fracture. Furthermore, because the normal fracture region typically experiences higher stress triaxiality, its voids have greater expansion rates and reach critical size first, making it the crack initiation zone during high-temperature tensile fracture.

Conclusions

1. The microstructure of the new corrosion-resistant X-2# alloy welding joint consists of single-phase austenite. The weld zone exhibits a continuous cooling cast structure with numerous equiaxed crystals in the weld remelting zone. The fusion zone shows a smooth transition from base metal to weld metal, and the heat-affected zone displays no significant grain coarsening.

2. The Vickers hardness of the X-2# alloy base metal is greater than that of the weld zone, which represents the softest region. However, the hardness of the weld remelting zone exceeds that of both front and back weld zones and approaches the base metal hardness.

3. From room temperature to 700 °C, the tensile strength of the welding joints is lower than that of the base metal, with a welding coefficient greater than 88.1%. The joint strength and weldability remain stable and can meet the requirements for service under supercritical conditions.

4. With increasing tensile test temperature, the fracture surfaces at 20, 300, and 400 °C show dimpled ductile fracture morphologies with shallow, small dimples and relatively low ductility and toughness. At 500, 600, and 700 °C, the fracture surfaces exhibit mixed ductile fracture morphologies consisting of dimples and tear ridges, with numerous tear ridges indicating good high-temperature strength. The fracture mechanism is a mixed mode of normal fracture and shear fracture.

References

[1] Ding Z H. Organic Wastewater Treatment Technology and Its Application. Beijing: Chemical Industry Press, 2002: 1 (丁忠浩. 有机废水处理技术及应用. 北京: 化学工业出版社, 2002: 1)
[2] Ma C Y, Zhao X C, Zhu F L, Guo K Q, Wu R X. Modern Chem Ind, 2007; 27: 497 (马承愚, 赵晓春, 朱飞龙, 郭凯琴, 吴荣霞. 现代化工, 2007; 27: 497)
[3] Zhang P, Wang J C, Zhang X D, Liu X W, Xia Y J, Li Z Y. Environ Prot Sci, 2003; 29(5): 15 (张平, 王景昌, 张晓冬, 刘学武, 夏远景, 李志义. 环境保护科学, 2003; 29(5): 15)
[4] Zhu F W, Zhang L F, Qiao P P, Liu R Q, Bao Y C, Chen Y Q. Nucl Power Eng, 2009; 30(5): 62 (朱发文, 张乐福, 乔培鹏, 刘瑞芹, 鲍一晨, 陈宇清. 核动力工程, 2009; 30(5): 62)
[5] Kritzer P. J Supercrit Fluids, 2004; 29: 1
[6] Was G S, Ampornrat P, Gupta G, Teysseyrea S, Westa E A, Allenb T R, Sridharanb K, Tanb L, Chenb Y, Renb X, Pister C. J Nucl Mater, 2007; 371(1-3): 176
[7] Yin K J, Qiu S Y, Tang R, Zhang Q, Zhang L F. J Supercrit Fluids, 2009; 50: 235
[8] Tan L, Ren X, Allen T R. Corros Sci, 2010; 52: 1520
[9] Ampornrat P, Was G S. J Nucl Mater, 2007; 371(1-3): 1
[10] Chen Y, Sridharan K, Allen T R. Corros Sci, 2006; 48: 2843
[11] Tan L Z, Yang Y, Allen T R. Corros Sci, 2006; 48: 4234
[12] Tan L Z, Yang Y, Allen T R. Corros Sci, 2006; 48: 3123
[13] Wright L G, Dooley R B. Int Mater Rev, 2010; 55: 129
[14] Sun C W, Hui R. Corros Sci, 2009; 51: 2508
[15] Chen Y, Sridharan K, Ukai S, Allen T R. J Nucl Mater, 2007; 371: 118
[16] Cho H S, Kimura A. J Nucl Mater, 2007; 367-370: 1180
[17] Isselin J, Kasada R, Kimura A. Corros Sci, 2010; 52: 3266
[18] Siwy A D, Clark T E, Motta A T. J Nucl Mater, 2009; 392: 280
[19] Zhu F W, Zhang L F, Tang R, Qiao P P, Liu R Q. At Energy Sci Technol, 2009; 43(6): 39 (朱发文, 张乐福, 唐睿, 乔培鹏, 刘瑞芹. 原子能科学技术, 2009; 43(6): 39)
[20] Was G S, Teysseyre S, Jiao Z. Corros, 2006; 62(11): 989

[21] Sun M C, Wu X Q, Han E H, Rao J C. Scr Mater, 2009; 61(10): 996
[22] Halvarsson M, Tang J E, Asteman H, Svensson J E, Johansson L G. Corros Sci, 2006; 48: 2014
[23] Tan L, Ren X, Sridharan K, Allen T R. Corros Sci, 2008; 50: 3056
[24] Sun M C, Wu X Q, Zhang Z E, Han E H. J Supercrit Fluids, 2008; 47: 309
[25] Zhang Q, Tang R, Yin K J, Luo X, Zhang L F. Corros Sci, 2009; 51: 2092
[26] Bao Y C. Master Thesis, Shanghai Jiao Tong University, 2011 (鲍一晨. 上海交通大学硕士学位论文, 2011)
[27] Dupont J N, Lippold J C, Kiser S D. Welding Metallurgy and Weldability of Nickel-base Alloys. Hoboken: John Wiley & Sons, Inc, 2009: 47
[28] Sima A P. Master Thesis, Shanghai Jiao Tong University, 2009 (司马爱平. 上海交通大学硕士学位论文, 2009)
[29] Zheng C Q, Zhou L, Zhang K S. Study on Mechanical and Its Application to Mesoscopic Metal Ductile Damage. Beijing: National Defence Industry Press, 1995: 27 (郑长卿, 周利, 张克实. 金属韧性破坏的细观力学及其应用研究. 北京: 国防工业出版社, 1995: 27)
[30] Zhao B H, He L, Yao Y M. Welding Processing Technology and Quality Testing, Failure Analysis and Metallograph Practical Handbook. Beijing: Metallurgical Industry Press, 2006: 1203 (赵炳辉, 何伦, 姚一鸣. 焊接件加工处理工艺与质量检测、失效分析技术及金相图谱实用手册. 北京: 冶金工业出版社, 2006: 1203)